

Chapter 12

SEQUENTIAL NUCLEATION AND GROWTH OF COMPLEX NANOSTRUCTURES BY A TWO-STEP STRATEGY

Li Yang^{1,}, Paul W. May¹ and Lei Yin²*

¹ School of Chemistry, University of Bristol, Cantock's Close, Bristol BS8 1TS, United Kingdom.

² Department of Aerospace Engineering, University of Bristol, Queen's Building, University Walk, Bristol BS8 1TR, United Kingdom.

Abstract

Self-assembled nanostructures are new forms of materials which are interesting from a fundamental scientific perspective, as well as having many potential technological applications. It is believed that the ability of nanostructures to self-assemble with controlled crystalline orientation, size, complexity and crystal morphology, provide potential applications in data storage, functional devices, communications and technology. Recently, a two-step strategy was successfully developed in our lab to produce two-dimensional or three-dimensional carbon nitride well-defined hierarchical complex structures. This strategy is a combination of a novel laser-induced deposition technique followed by self-assembly. In the first step, a suspension of carbon nitride nanoparticles was prepared by liquid-phase pulsed laser ablation (LP-PLA). In the second stage, this suspension was deposited onto a silicon substrate to act as a 'seed' layer. Via controlling the rate of evaporation of the liquid phase part of the seed suspension, and the size and the quantity of nanocrystals within the droplet, it was possible to create a range of nanoscale structures, including dense nanospheres, highly-symmetric flowers, hollow core-shell and uniform grass-like structures. The growth of such complex structures is governed by an evaporation-driven self-assembly process. As the droplet dries, small building blocks, such as nanoparticles (NPs) or nanorods (NRs) nucleate upon the existing crystals and template, sharing the same edges, to form a close-packed arrangement. By varying the design of the building blocks, materials combination, interfacial chemistry, and confining dimensions, it is expected to extend this synthetic approach to a range of new structured materials with useful functional properties.

1. Introduction

Self-assembly is an incredibly powerful concept in modern molecular science. The ability of carefully designed building blocks to spontaneously assemble into complex nanostructures underpins developments in a wide range of technologies — from materials science through to molecular biology. Due to the multi-disciplinary nature of this new subject, the definition of a self-assembling process may be different among researchers from different fields. Generally speaking, self-assembly is a process in which components, either separately or linked, spontaneously form ordered aggregates [1]. The interactions involved usually are non-covalent, such as electrostatic interactions, hydrogen bonds, van der Waals' forces, coordination interactions and hydrophobic effects [2]. In self-assembled structures, these intermolecular forces connect the molecular building blocks in a reversible, controllable and specific way. Of particular value are the possibilities offered by self-assembly to generate nanoscale complexity with relatively little synthetic input. Furthermore, the ability of assembled superstructures to behave as more than the sum of their individual parts, and exhibit completely new types of behaviour, is of special interest [3].

Due to the emergence of a new generation of high-technology materials, two-dimensional (2D) and three-dimensional (3D) self-assembled, aligned nanomaterials have begun to be widely investigated over the last decade [4,5]. It is believed that the ability of nanostructures to self-assemble with controlled crystalline orientation, size, complexity and crystal morphology provide potential applications in data storage, functional devices, communications and technology. As a result, a rapidly growing field of science has emerged to understand and control these self-organized architectures, involving the dedicated efforts of chemists, physicists, material scientists and biologists. In general, physical methods (including chemical vapour deposition [6], vapour phase transport [7], and pulsed laser ablation in vacuum [8]) and chemical methods (including hydrothermal methods [9], soft-template [10] and use of various surfactants [11,12]) have been developed to fabricate nano- to microscale materials with a range of morphologies, such as compact hexagonal networks [13], rings [14], dandelion-shaped hollow structures [15], strips [16], tubes [17], and flower-like structures [18]. For example, ZnO forms micron- and submicron-scale 'dandelion'-like structures, which are comprised of single-crystalline building units (either nanorods (NRs) or nanoparticles (NPs)) [19], and which can be constructed via a modified Kirkendall process in solution, where the pre-formed oxide layer serves as a shell template for the initial nucleation and growth. Also, uniform Sb_2S_3 bundles coalesced from numerous NRs have been synthesized on a large scale using a hydrothermal technique at a temperature of 180°C for 20 h [20]. However, it is well known that these physical techniques require relatively high temperature, vacuum conditions, and expensive equipment, or sometimes complicated processes, which limit them to smaller scale fabrication. Also, conventional chemical methods usually involve the use of catalysts, surfactants and possibly complex chemical reactions, which often produce a significant amount of unwanted byproducts requiring further purification. Therefore, a technique which combines the merits of both physical and chemical methods, while giving high yield at low cost, would be desirable, if novel self-assembled materials are to be produced on an industrial scale.

One such technique, liquid-phase pulsed laser ablation (LP-PLA), has only relatively recently been applied to produce self-organized nanomaterials [21,22,23]. Details about the

technical aspects of LP-PLA can be seen in a recent review by Yang [24] who gives comprehensive details of the nucleation thermodynamics, the phase transition, and the growth kinetics of nanocrystals by laser ablation of liquids. Briefly, LP-PLA involves focusing a high power laser beam onto the surface of a solid target, which is submerged beneath a liquid. The interaction of the laser with the target causes the surface to vaporise in the form of an ablation plume, which contains species such as atoms, ions, and clusters, travelling with high kinetic energy. The species in the plume collide and react with molecules of the surrounding liquid, producing new compounds containing atoms from both the original target and the liquid. Due to the intensity of the laser and the nanosecond timescales, the instantaneous temperatures and pressures within the reaction volume can be extreme (many thousands of K at tens of GPa) [25]. Such high temperature, high pressure, and high density conditions provide a 'brute force' method of synthesising novel materials that have hitherto been inaccessible using milder, more conventional techniques.

Extensive progress has been made towards the production of many types of inorganic nanoparticles, including metals, metal oxides, and other semiconductors [26]. However, to date, research on the understanding of the self-assembly processes of Group IV-V compounds, such as carbon nitride, is still in its infancy, and synthesis of complex nanostructures has only just begun. Carbon nitride has been the subject of numerous publications since the prediction by Liu and Cohen [27] in 1989 that crystalline C_3N_4 should have superhard properties. However, a successful synthesis of bulk amounts of this material still remains a challenge. The synthesis difficulties are due to its low thermodynamic stability and complex bonding environment. Recently Li and co-workers [28] demonstrated a range of self-assembled carbon nitride morphologies (including nanotube bundles, aligned nanoribbons and microspheres) could be prepared by a solvothermal technique. Also, our recent findings [29,30] indicated that the instantaneous high temperature, high pressure and high density conditions that arise when a high-intensity focused laser beam impinges upon a graphite target confined by a thin layer of liquid ammonia can promote growth of crystalline carbon nitride NPs. In this chapter, we will further demonstrate a successful synthesis of carbon nitride hierarchical nanostructures via a two-step strategy, whereby the nanocrystals self-assemble into complex 2D or 3D superstructures. Fabrication of these carbon nitride structures from small building blocks via self-organization suggests that the chemical and physical properties of these superstructures are intrinsic to the self-assembly induced by the close vicinity of the NPs or NRs. Finally, a summary and expectation are discussed with regard to the application of LP-PLA as a synthesis route for highly desirable complex architectures.

2. Processing Hierarchically Structured Nanomaterials

Production of zero-dimensional (0D) NPs and one-dimensional (1D) nanocrystals by laser ablation in liquid media has been extensively studied [31,32,33]. Since the 0D and 1D nanocrystals can serve as building blocks in forming 2D or 3D complex architectures with long-term periodic structures, it should be expected that the LP-PLA approach would have great potential as a means to grow large arrays of hierarchical, complex, oriented and ordered superstructures. Extending this concept, we performed a two-step synthesis to produce oriented carbon nitride nanostructures based on previous results [21, 22].

In a typical synthesis process, the carbon nitride seed solution was initially prepared by LP-PLA. Briefly, a solid graphite target (Testbourne Ltd., 99.99%) was ablated at room temperature while submerged in a 5 ml solution of 25-35% ammonia solution (Fisher Scientific, used as received without further purification) inside a sealed stainless steel cell. In order to reduce the effect of target aging, the cell was rotated at 700 r.p.m. during ablation using a standard magnetic stirrer. A Q-switched Nd:YAG laser (532 nm, pulse duration 15 ns, frequency 10 Hz) was directed by a prism and then focused onto the graphite surface using a 25 mm-focal-length lens. The intense laser light passed through a quartz window in the top of the cell, then through ~5 mm layer of the liquid covering the graphite, to form a ~0.5 mm-diameter spot on the target surface. The ablation was typically carried out at laser fluences of 25-125 mJ / pulse for reaction times $t = 0.5-24$ h. After ablation, a pale yellow colloidal suspension was obtained, which contained a mixture of unreacted graphite and ablation product, both in the form of NPs. The suspension was stable, with no precipitate being observed for months or even longer. The graphite sediments were filtered and removed as much as possible by boiling with 70% perchloric acid, before further characterization. For the second step, a few drops of this seed suspension was deposited onto a 1 cm \times 1 cm silicon p-(100) substrate and the liquid allowed to dry. Many more complex nanostructures than the simple NPs and NRs can be produced in a controlled fashion by simply altering the drying time and drying method of the suspension of ablated product. Four different drying processes were used in the present study: (1) dry naturally in air; (2) dry in a sealed tube; (3) dry rapidly in an oven or on a hotplate; (4) dry in a critical point dryer (CPD). Those procedures allowed the time taken to evaporate the liquid to be controlled.

For materials analysis, a drop of the suspension was deposited onto a silicon p-type (100) substrate or transmission electron microscopy (TEM) grid, and then allowed to dry. The product was characterized using X-ray diffraction (XRD; Bruker-AXS D8 powder diffractometer, Cu K α radiation), field emission scanning electron microscopy (FE-SEM; JEOL 6300 F), TEM (JEOL 1200 EX, 120 kV), high-resolution (HR) TEM (JEOL 3000F, 300 kV) and energy-dispersive X-ray analysis (EDX). X-ray photoelectron spectroscopy (XPS; Thermo VG Scientific), laser Raman spectroscopy (Renishaw 2000, excitation wavelength 325 nm) and Fourier-transform infrared spectroscopy (FTIR; using a KBr disc) were performed to search for evidence of C-N, C=C and C \equiv N bonds.

3. Sequential Nucleation and Growth of Complex Nanostructures

3.1 General Structure of the Nanocrystal Self-assembly

All reported samples in the present work were first examined with XRD, EDX, Raman and XPS techniques to obtain their crystallographic structure and chemical composition. Experimental details of the procedures can be seen in our previous reports [21, 22, 23].

Studies performed at various conditions showed that factors such as ablation time, laser energy, ammonia concentration and the drying speed were important in order to obtain organized assemblies of NPs. By depositing the carbon nitride seed solution onto a silicon substrate and controlling the drying process under different conditions, four main classes of structure were identified in the ablation product, categorised as Types I-IV based upon their

shape and size (Figure 1(a)). The first class of structure (Type I) had the shape of thin plates with rounded edges. Since they were the components of the larger ‘flower-like’ structures (described later), they have been termed ‘nano-petals’. The quantity of these nano-petals and their location with respect to the larger structures (see later) were dependent upon the deposition and drying conditions. As shown in Figure 1(b-c), this indicated that these nano-petals were 2D crystallites of carbon nitride which preferentially aligned themselves perpendicularly to the surface of the Si substrate. The number and length of these nano-petals increased with increasing laser ablation time from 0.5 to 2 h for the same laser fluence. X-ray diffraction (XRD) analysis (spectrum not shown here) of these nano-petals showed that they were crystalline, and all the diffraction peaks were consistent with ($h00$) preferential orientation [29].

The crystallographic information was indexed to hexagonal β - C_3N_4 ($P6_3/m$ (176)) with lattice constants $a_0 = 6.4017 \text{ \AA}$ and $c_0 = 2.4041 \text{ \AA}$ [34]. Interestingly, it is also possible that these nano-petals began to aggregate and self-assemble (Figure 1(d)). When the concentration

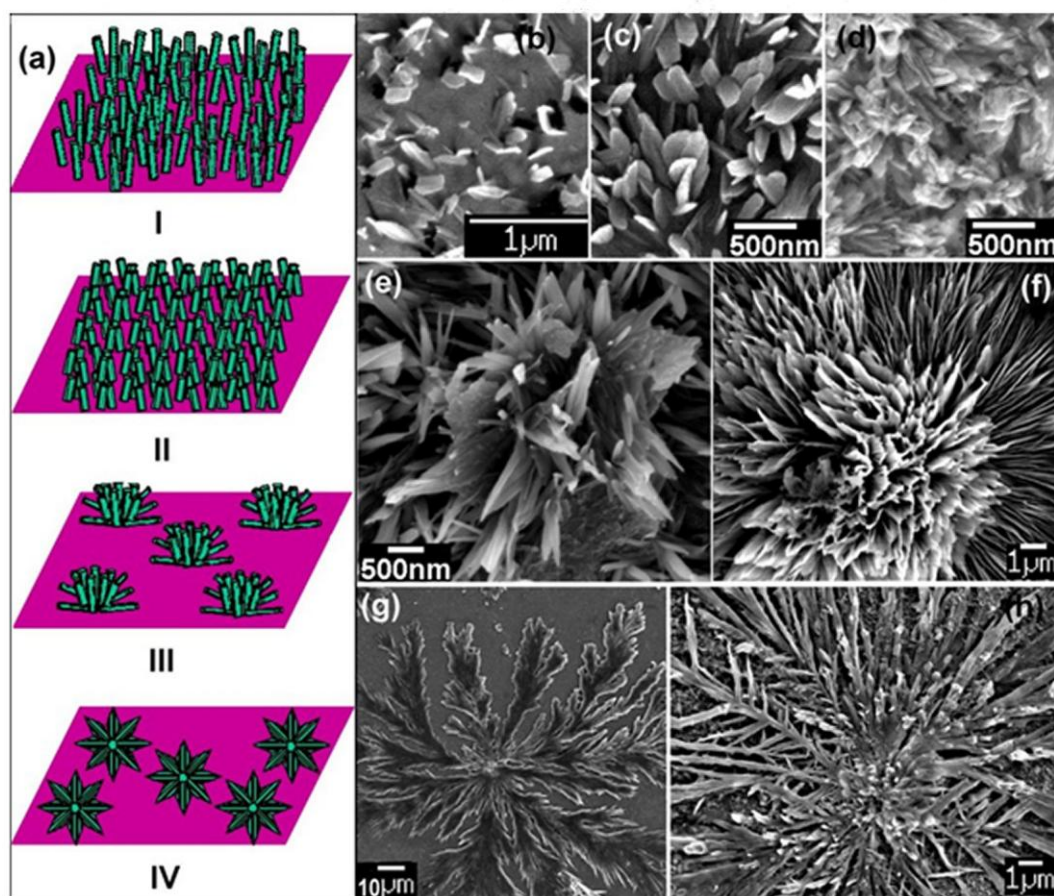


Figure 1. (a) Schematic illustration of the growth process leading to the observed four main classes of hierarchical structures, labelled I to IV. (b)-(d) Scanning electron microscopy (SEM) images of carbon nitride ‘nano-petals’ following ablation times of: (b) 0.5 h, (c) 2 h, and (d) 3 h. (e-f) Overall ‘flower-like’ structure following 5 h laser irradiation (synthesis conditions: laser power 125 mJ, 35% ammonia solution, drying in air). (g-h) 2D flattened flower, sample conditions identical to (e-f) except it was dried on a hotplate at 200°C (g) and an oven 80°C (h). (Reproduced from [29])

by the permission of Royal Society of Chemistry (RSC) and [30] by the permission of Nova publishers).

of nano-petals in the suspension increased, they tried to minimize their interfacial energy upon subsequent drying of the liquid by preferential tilting with respect to each other. This produced the second class of nanostructure (Type II), which has a 'grass-like' shape and exhibits several different morphologies (see later discussion). However, all are produced in large quantities and cover the whole substrate.

By carefully controlling the drying process, 'flower-like' spiked, crystalline superstructures were formed (Figure 1(e-f)). This third class of structure (Type III), now fully 3-dimensional, with sizes 1-20 μm , were created when many nano-petal structures coalesced at a common centre with multi-fold symmetry. One possible explanation is that the presence of the solid substrate physically hinders growth in that direction; so many branches are tilted away from the substrate, towards the solution.

When the evaporation speed of the liquid was rapid (for example, drying in an oven or hotplate), a fourth class of structure (Type IV) was observed (Figure 1(g-h)). Instead of 3D flowers, the carbon nitride now formed 2D 'star-like' or flattened flower-like structures. New dendrites emanated from the core and acted as nucleation centres, eventually allowing the structure to expand into 2D horizontal flowers (Figure 1(h)). It is suggested that the higher water evaporation rate increased the interparticle capillary forces [35]. As the continuous flux of particles filled up the spaces on the substrate, successive layers would be formed rather than 3D complex shapes.

Although these four types of structures have different densities and morphologies, they all exhibit high surface-to-volume ratios and so might have potential in semiconductor devices, anticorrosion protective coatings and new applications.

By controlling the solution evaporation rate on a carbon-coated TEM copper grid (as our substrate), different final complex architectures could be also achieved on various length scales. If the droplet dried in air (less than 1 h), the structure had the shape of nearly monodispersed spheres with rounded edges (Figure 2(a)). Those spheres have very high density and are close-packed. When increasing the laser fluence and ablation time, the nanostructure resembles 'flower-like' spiked crystallites (Figure 2(b)) for the same drying speed, where the NRs have coalesced at a common centre with multi-fold symmetry. It seems that these flower-like structures are simply less dense versions of the spheres (Figure 2(c)), with numerous voids between the NR framework comprising the flowers. Similar interior space would be eventually generated within the solids, as the smaller NPs are undergoing mass transport throughout the prolonging drying times (Figure 2(d)). The solid carbon nitride flower (similar to that in Figure 2(b)) has become hollow (named 'hollow-flowers'), which divided the pristine solid sphere into two discrete regions and formed a core-shell structure. In these structures, the NPs remain loosely attached to the outside, forming the interconnected void space, although the interior vacant volume might vary in each individual hollow-flower (for instance the interior void space size is in order: 1st > 2nd > 3rd > 4th, as shown colour contrast for two discrete regions of individual hollow-flower in Figure 2(d)). It is worth pointing out that by simply altering the drying time and drying method of the suspension, the final morphology can exhibit semi-hollow, core-shell, or even full-hollow structures. These observations are similar to the report by Liu and Zeng [36], who demonstrated the fabrication of ZnS nanomaterials with hollow interiors. Yang and Zeng also reported a simple approach

to prepare hollow TiO_2 nanospheres with highly organized crystallites in the shell structure and surface regions [9].

Compared to the flower-like structures, the hollow-flowers are less common. A longer drying time in an above-ambient temperature aids the small crystallites to move freely in the solution enabling oriented aggregation. The relative ratios the nanosphere, nanoflower and hollow-flower structures are approximately 30%, 60%, and 10%, respectively (based on a total of 800 TEM images), noting that the statistical ratios vary for different experimental conditions. In general, a higher synthetic energy (*i.e.* high laser power, long ablation time, high ammonia concentration and long drying time) leads to better crystallinity, but larger size for the products.

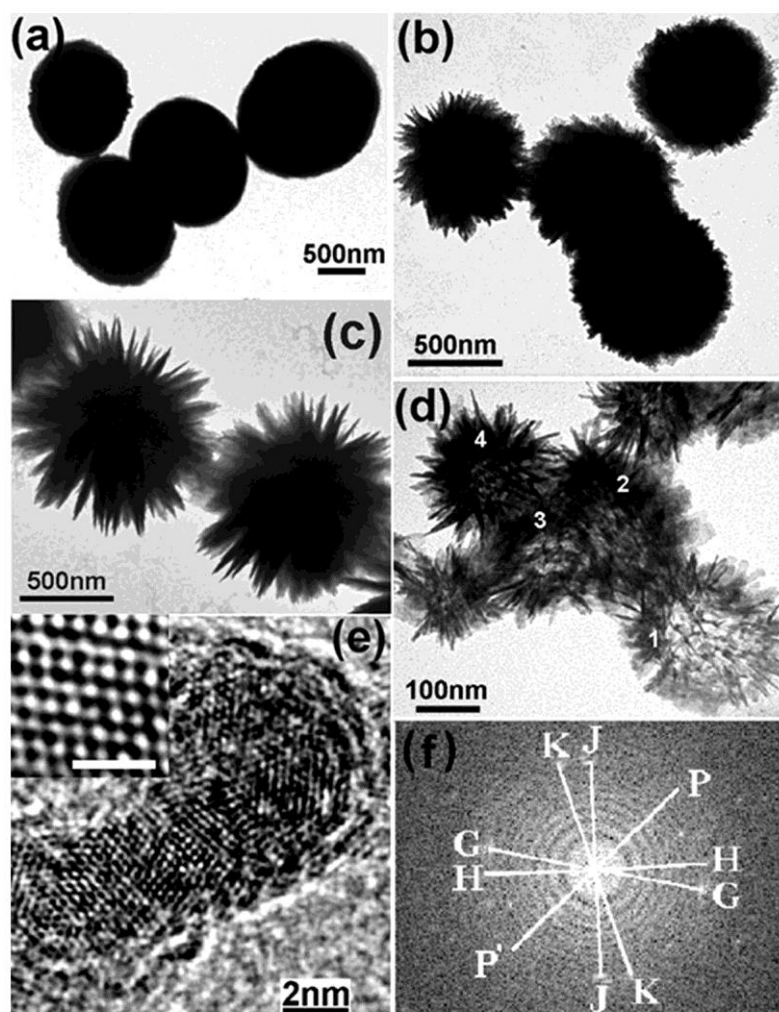


Figure 2. (a) Nanospheres with rounded edges (synthesis conditions: laser power 50 mJ, ablation time 2 h, 35% ammonia solution, drying in air). (b-c) Nanoflowers with numerous protruding spiky surfaces (synthesis conditions: laser power 100 mJ, ablation time 8 h, 35% ammonia solution, drying in air). (d) Hollow-flowers with tunnels connecting from the centre to the outward shell (synthesis conditions: laser power 100 mJ, ablation time 10 h, 35% ammonia solution, drying in a sealed tube). The numbers denote the individual hollow-flower. (e) HR-TEM image of a single NR, the inset shows the atomic arrangement and scale bar 1 nm. (f) The Fourier-Filtered Transform (FFT) pattern corresponding to the

region shown in (e). K, J, H, G, P and P' label the positions of the six domains (see text for details). (Reproduced from [23] by the permission of Institute of Physics (IOP)).

In principle, assembly is energetically favoured because the formation of larger crystals can greatly reduce the interfacial energy of isolated NPs or NRs. Therefore, most of our final products are either well-defined nanosphere structures or self-assembled flower-like architectures if the TEM grid dried naturally in air. Only occasionally were monodispersed NPs or isolated NRs seen by TEM. The mechanism for how these lower dimensional building blocks construct to higher dimensional arrangements, rather than random clumps, is still unclear. However, the above evidence indicates that 'oriented attachment' [37] was observed among the crystallites, in which a larger crystal structure is formed from smaller ones by direct joining of suitable crystal planes. In particular, in the HRTEM image of Figure 2(e) taken from a single NR, the periodic lattices show the atomic arrangement (Figure 2(e), inset) with very few defects, and reflect the relationship between the orientation of the NPs and the crystallography of the ordered NR array. The corresponding Fourier-Filtered Transform (FFT) pattern illustrates that the nanocrystal consists of six domains with sixfold twins. The split spots K and J, H and G in the FFT pattern is due to the small angle between the twin boundaries. The reflections P and P' in Figure 2(f) are not split, and represent the coherent positions of the twin boundaries.

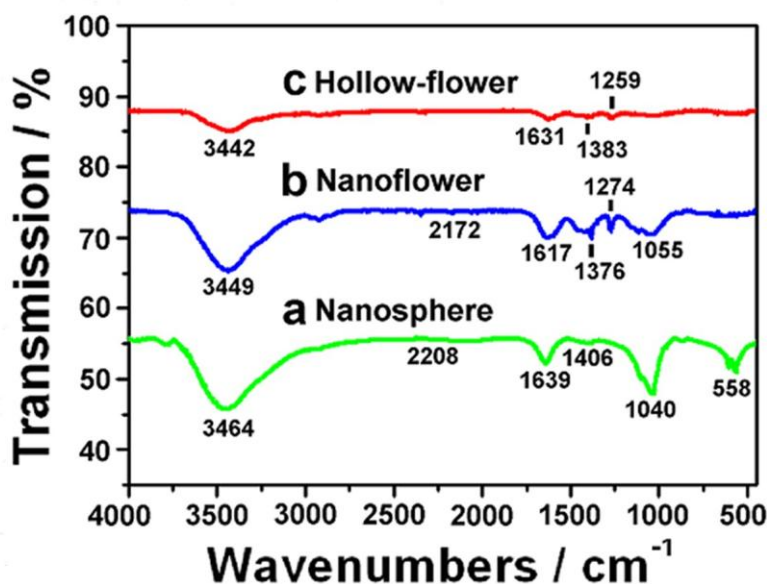


Figure 3. FTIR spectra of three different carbon nitride structures: (a) nanosphere, (b) nanoflower, (c) hollow-flower. (Reproduced from [23] by the permission of Institute of Physics (IOP)).

Information regarding the chemical bonding structure was obtained from Fourier transform infrared spectroscopy (FTIR). Figure 3 shows the FTIR spectra of the above-mentioned different morphology of carbon nitride crystals, which exhibits several peaks related to the chemical bonding between carbon and nitrogen [38]. The region $1000\text{--}1500\text{ cm}^{-1}$ corresponds to C-N single bonding, while the regions $1500\text{--}1750\text{ cm}^{-1}$ and $2150\text{--}2300\text{ cm}^{-1}$ are related to C=N and C≡N bonding, respectively. Similar spectra were also obtained by

Zimmerman and co-workers [39]. In our case, for the nanosphere structures (Figure 3(a)) the two peaks at 1040 cm^{-1} and 1406 cm^{-1} correspond to the C-N stretching mode. The absorption band at 1639 cm^{-1} is assigned to the stretching vibrational modes of C=N. Moreover, a small peak at 2208 cm^{-1} can probably be attributed to C \equiv N bonds, although it is much weaker compared with the other stretching modes. A broad band centred at 3464 cm^{-1} is due to NH group vibrations [40]. The 558 cm^{-1} peak can be assigned to the out-of-plane bending mode for graphite-like sp^2 domains, which become IR active due to nitrogen incorporation into the bonding network. The obvious differences between these samples are that the intensities of all the features are weaker and broader for the nanoflower and hollow-flower shape nanostructures. We attributed this to the voids in the nanoflowers and the internal nanospaces existing in the hollow-flowers.

3.2. Control of the Quality of Self-assembly

3.2.1. Diffusion of the Building Blocks

Usually, ordered organization was obtained following evaporation of a drop of a nanocrystal solution that had been deposited onto a TEM grid. Figure 4(a) shows a typical symmetric carbon nitride ‘flower’ together with its nano-petal building blocks (which look like flattened rods in the TEM). Figure 4(b) shows that these nano-petals appear fused together and ‘interwoven’ to form a lattice-like framework of the flower-like superstructure. The figure also shows the NPs that surround each nano-petal, and which fill in the holes within the framework to produce a dense, solid structure. EDX analysis confirms that carbon and nitrogen are present in all these structures, and micro-diffraction pattern (MDP, Figure 4(c)) was also consistent with crystalline hexagonal β -phase carbon nitride oriented along the [001] zone-axis. Several [001] patterns in Figure 4(c) can be identified at the same time, indicating that the nano-petals consist of several domains, with different rotational orientations contributing to the diffraction pattern. The HR-TEM image in Figure 4(d) shows that the nano-petals at the very edge of the flower contain very few defects and are single crystalline, as was anticipated from the MDP. Again, the lattice fringes ($d_{200} = 0.28\text{ nm}$, $d_{140} = 0.15\text{ nm}$) and their angles (106°) are in good agreement with the calculated values for hexagonal β -C $_3$ N $_4$ [41].

The smaller NPs, which lie in and around the nano-petal-framework comprising the flowers, appeared to be mobile with respect to this framework, and diffused outward from the centre of the flower with longer drying times. The results of this diffusion can be seen in Figure 4(e), where the solid carbon nitride flower (similar to that in Figure 4(a)) has become hollow. The NPs have diffused from the centre but remain loosely attached to the outside, making the outer shell of the flower appear fuzzy. The thickness of the fuzzy shell was $\sim 140\text{ nm}$ and that of the hollow core was $\sim 200\text{ nm}$ (shown as a lighter colour in the image). When the suspension was placed onto a hot-plate at 200°C for 0.5 h, the hollowing process was accelerated to form a semi-core-shell structure. The radial distribution of the NRs formed channels leading from the centre to the shell (Figure 4(f)). Another type of hollow structure was observed when the core-shell structures were essentially separated by a hollow tunnel, without linkage to the sphere (Figure 4(g)).

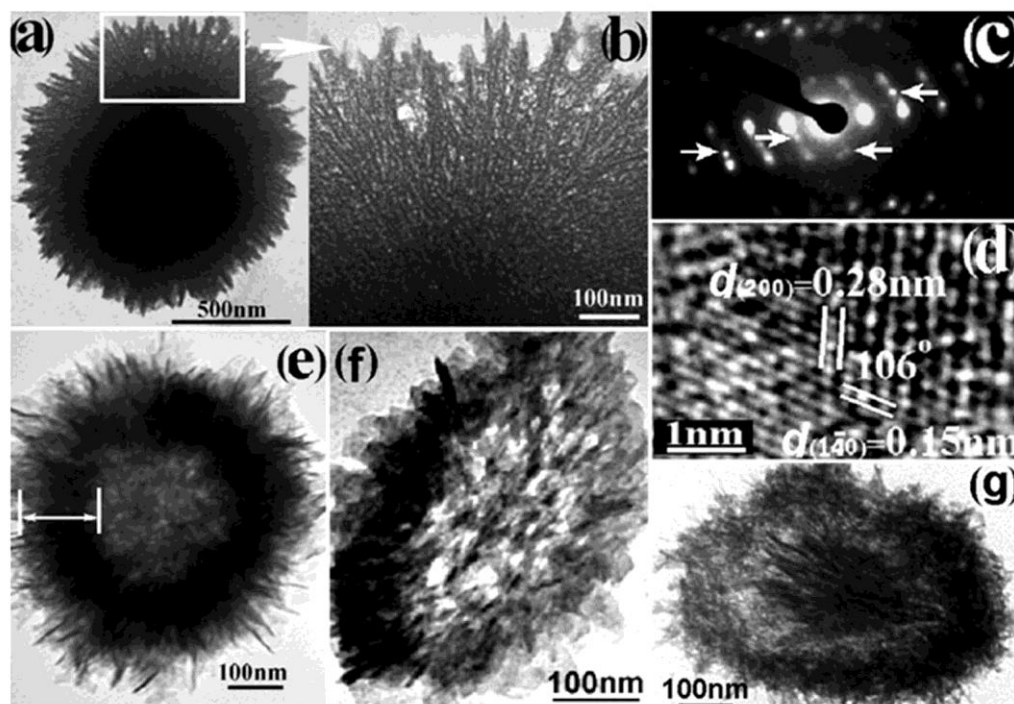


Figure 4. TEM image of the flower-like structures produced by LP-PLA of a graphite target in 35% ammonia solution (laser fluence 125 mJ/pulse) for 5 h. (b) A higher magnification image of the framed region in (a), showing a high density of NPs surrounding the nano-petal framework. (c) [001] zone-axis MDP from the tips of the nano-petals in (b), which corresponds closely to the calculated interlayer d -spacing of β - C_3N_4 . Arrows point to different sets of [001] reflections (see text). (d) HR-TEM image recorded from the edge of the flower nanostructure that is oriented along [001]. (e) TEM image of a hollow flower formed after 8 h LP-PLA and prolonged drying. (f) Semi core-shell structure. (g) core-shell structure with a hollow tunnel. (Reproduced from [29] by the permission of Royal Society of Chemistry (RSC)).

§ 3.2.2. Interconnection between the Big Structures

Self-assembly normally occurs when nanoscale objects interact with one another through a balance of attractive and repulsive interactions. If the attractive force is dominant, the components may interconnect and form larger aggregates. In contrast, the exterior appearance of the interlinked nanostructures did not change appreciably when the interaction was weak. It was found that the interconnections among the structures were different. Figure 5 shows two examples of these cluster-like combinations, for nanospheres and nanoflowers. Figure 5(a) shows a single, typical nanosphere with a dense surface, similar to those mentioned previously in Figure 2(a). Figure 5(b-c) shows that two neighbouring spheres can be fused together, or just joined loosely via their outside edges, with no change of internal structure. However, for the nanoflowers, the situation was different. Figure 5(e) shows that when two nanoflowers fuse, the inner spaces between the NRs were integrated throughout the entire cluster structure. One important note is that the fusing together of pristine nanoflowers alters the crystalline size slightly (~ 800 nm in diameter) but the morphology of nanoflower remained (Figure 5(f)).

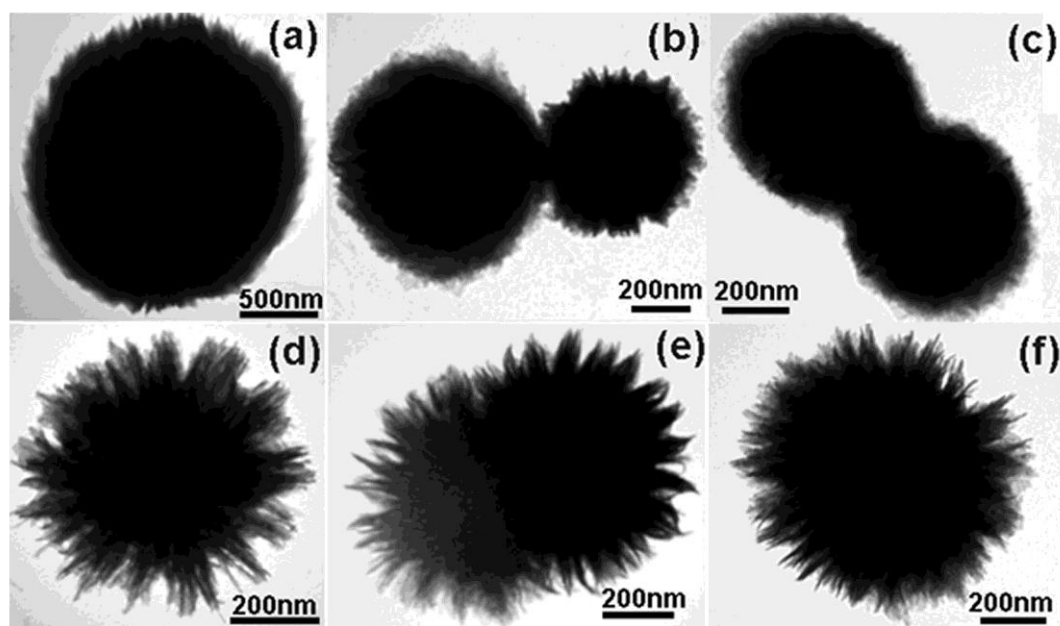


Figure 5. Examples of coalescence (eventually leading to clustering) of dense carbon nitride nanospheres and porous nanoflowers. (a) A single nanosphere, (b) 2 nanospheres touching, (c) 2 nanospheres fused together. (d) A single nanoflower, (e) 2 nanoflowers partially fused together, (f) 2 nanoflowers completely fused.

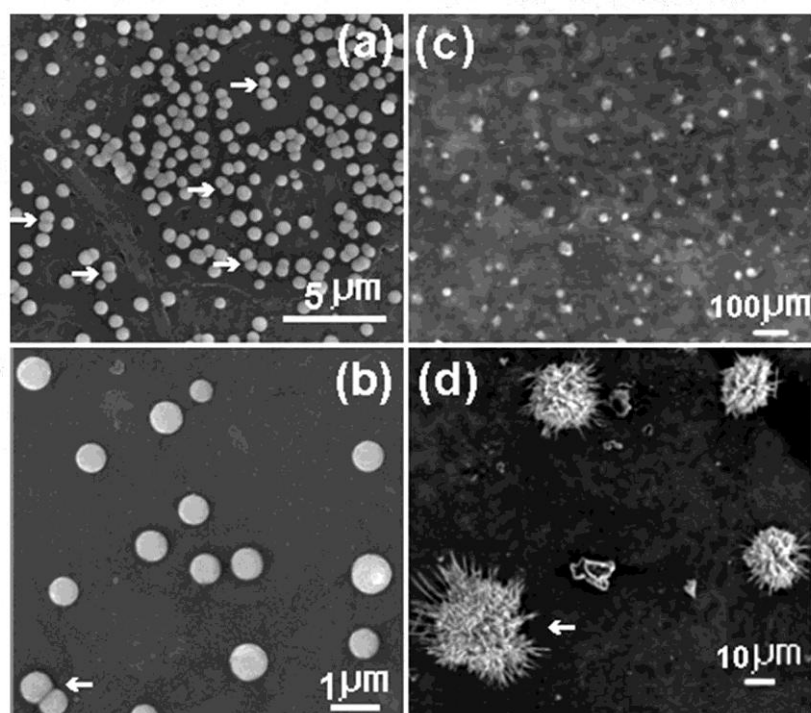


Figure 6. (a-b) nanospheres (carbon nitride seed solution is identical to that used for Figure 2(a)). The fused nanospheres are marked by arrows. (c-d) nanoflowers (carbon nitride seed solution is identical to Figure 2(b-c)). The drying process was in air. The arrow in (d) shows possible fused nanoflowers. Note that image (b) and (d) are recorded in higher magnification from (a) and (c), respectively.

If the TEM grid was replaced by a silicon substrate, and the previously prepared carbon nitride seed suspension was applied and dried naturally in air, similar morphologies to those shown in Figure 5 were obtained. However, the nanospheres were now formed with a more uniform size distribution, as shown in Figure 6(a-b). Some nanospheres (size about 500 nm-1 μm) were attached with a boundary visible in between (highlighted by arrows for clarity). The interaction between such interconnected nanospheres is weak since they could be broken up with a few minutes' of sonication. In contrast, the nanoflowers were dispersed individually (Figure 6(c)) with a larger size distribution (\sim 1-15 μm). It is noted that the size of the nanoflowers found by SEM on the Si substrate appeared much larger than those under TEM observation (size about 500 nm-800 nm). This is probably due to some of the nanoflowers fusing together completely to produce larger, interlinked nanoflowers (see Figure 6(d), highlighted by the arrow). Such nanoflowers are stable and sustainable without any change even after a few hours' of sonication. The reason the nanoflowers fused more completely was to do with the different interaction between the particles within the seed suspension and the two types of substrate. The TEM grid was normally placed onto a filter paper and a drop of carbon nitride aqueous suspension was pipetted onto the grid. Due to the presence of the filter paper, water was quickly removed. For the SEM sample on a Si substrate, the droplet of suspension took at least 2 h to dry in air. This allowed sufficient time for the nanoflowers to aggregate. Further investigation needs to be carried out.

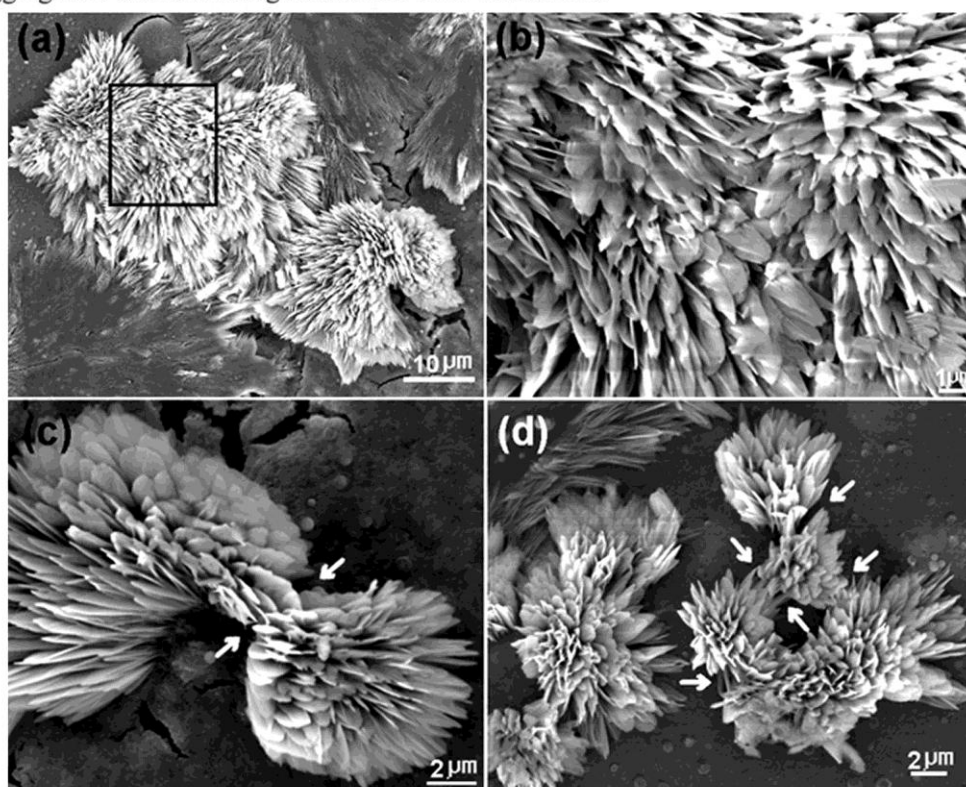


Figure 7. Fused-flower (carbon nitride seed solution is identical to that used in Figure 2(b-c)). Drying process is in a sealed tube (\sim 8 h evaporation). See text for discussion. Arrows in (c) and (d) are marked for clarity.

Control experiments provide some evidence to support this proposed mechanism. Under identical conditions, a droplet of carbon nitride suspension was deposited onto a Si substrate and placed into a sealed tube. The drying process was now estimated to be around 8 h. As expected, larger flowers constructed from hundreds of thin plates were formed (Figure 7(a)). Careful observation found that these larger flowers were actually an aggregate of more than one nanoflower. The boundary between the nanoflowers was perfectly fused and aligned. The enlarged region in Figure 7(a) marked by black box shows that numerous nanoplates are bunched up and cross-linked with recognizable boundaries or voids between the component subunits (Figure 7(b)), which are still maintaining their close proximity. Such results can be further seen in Figure 7(c-d). Occasionally, flowers were not fully developed, since the rate of aggregation among the nanoflowers varies depending upon local conditions. But the arrows marked in Figure 7(c-d) clearly indicate the fusion of the adjacent nanoplates. Given sufficient time (*e.g.* by prolonging the drying time), the growth of the flower will fully complete into three dimensions.

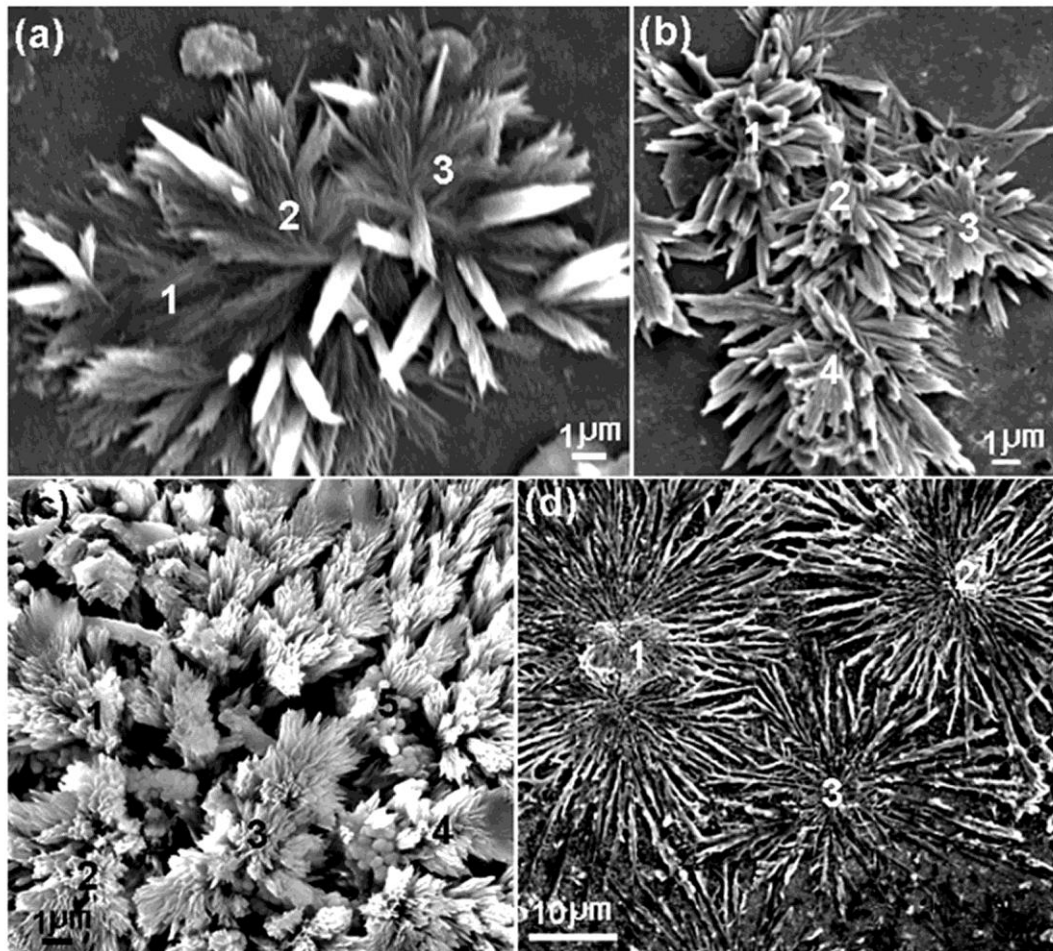


Figure 8. (a-b) 3D interconnected flowers. (c-d) 2D flattened flowers (synthesis conditions: 35% ammonia solution, laser power 100 mJ, 3 h ablation and dried in a sealed tube, (c-d) seed solution was diluted by using deionised water). Numbers in (a-d) denote the individual flower.

A few more examples of interconnection between larger complex structures are given in Figure 8. As shown in Figure 8(a), the neighboring 'long-petalled' crystals can further expand themselves and eventually merge into an interconnected structure [42]. At least 10 petals are needed to form the secondary flower-like architectures. Some of them sprouted out to three dimensions but some were lying down along the substrate (see 3rd flower in Figure 8(b)). However, when using diluted carbon nitride seed suspension, the morphology changes (Figure 8(c-d)) in the mesoscopic structure may be correlated to interactions between nanocrystals. The interconnection between those flowers was also observed, although the forces seemed weaker (larger voids exist, see the numbered regions in Figure 8(c-d) for demonstration) compared with those shown in Figure 7. The disappearance of the 3D structural dimension and the occurrence of 2D flattened flowers which cover the substrate are believed to be a result of a significant decrease in the interaction between the dispersed nanocrystals in the droplets. In a slow evaporation, the attractive force between NPs is low and they are likely to diffuse close to the substrate leading to formation of 2D flattened structures.

3.3. Dynamic Study of Self-assembly Formation

3.3.1. Influence of the Drying Time

Morphology development of the high-order grass-like architectures at different growth stages was monitored by SEM (Figure 9). The evaporation rate was controlled by either the substrate temperature or the solvent saturation degree of the surrounding atmosphere. The seed suspension used was spherical NPs with an average particle size of 15-20 nm under TEM observation (see Figure 9(a) inset). When a droplet of this suspension was deposited onto a silicon substrate and placed on a hot-plate, the solution dried quickly (about 30 min). In this case, the NP morphology remained, and small islands of NP aggregates dispersed on the surface sparsely (Figure 9(a)). In contrast, if the droplet on the Si substrate dried naturally in air (~2 h), 1D NR nuclei started branching on the surface and gradually formed 2D 'roots' (~200 nm in size), see Figure 9(b). If instead, the droplet dried inside a sealed tube (~8 h), the number of nanopetals increased and started interconnecting or aggregating (see the left side of Figure 9(c)). The 2D primary nanopetals took about 12 h to coalesce into grass-like structures (Figure 9(d)). Upon further increasing the drying time to 24 h, the NPs adjusted their position and continued to assemble, stem-like, and eventually expanded into fully-developed 3D architectures (Figure 9(e)). In the enlarged image of Figure 9(f), it can be seen that nanopetals on each side stem were nearly parallel to one another. Moreover, NR bundles can be clearly observed in each nanopetal (see the highlighted area in Figure 9(f)). It should be noted that such heterogeneous nucleation and growth in solution were not observed by means of TEM.

Similar experiments were also performed using the carbon nitride seed suspension produced by 35% ammonia solution, laser power 50 mJ, 12 h ablation. This produced nanoflowers which exhibited surfaces composed of NRs, where the NRs radiated outward from the centre, as shown in Figure 10(a) inset. The starting seed morphology was more complex than the NPs used in the previous time evolution study. Since it was observed that nanoflowers exhibited a surface composed of NRs, we expect that a similar morphology

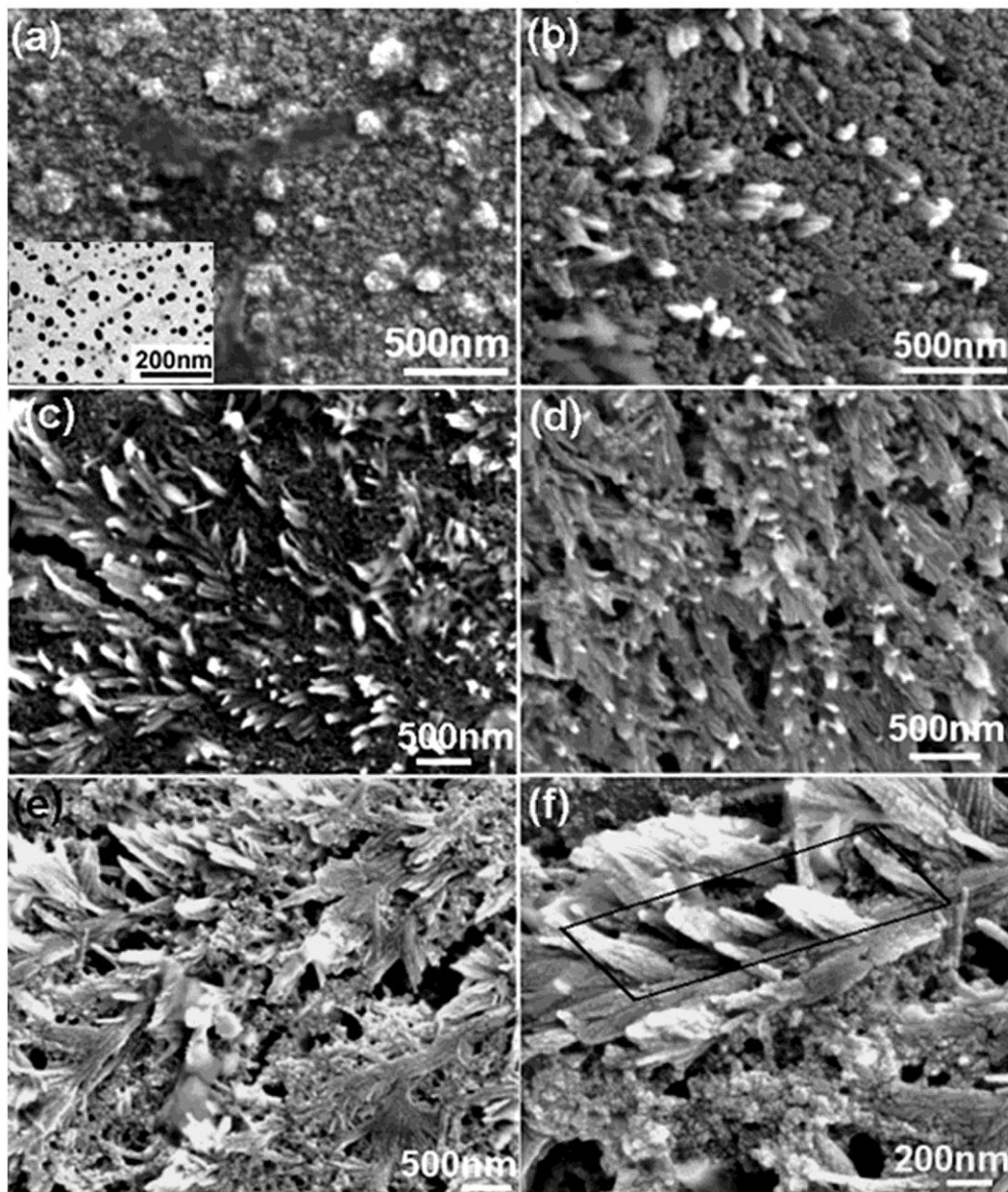


Figure 9. Time-dependent evolution of grass-like crystal morphology at different growth stages for (a) 30 min, (b) 2 h, (c) 8 h, (d) 12 h, and (e-f) 24 h, respectively. The box in (f) highlights the nanopetals arrangement. (Synthesis conditions: 35% ammonia solution, laser power 75 mJ, 10 min ablation, spherical NPs with an average particle size of 15-20 nm were used as seeds, as shown in Figure 9(a) inset. See text for discussion).

should appear on the Si substrate. However, no regular shaped objects were detected by SEM when the droplet was dried in air. Only some low contrast flower-shape patterns (Figure 10(a)) were seen which appeared uniformly dispersed. The enlarged image in Figure 10(b) shows that such patterns are actually formed by a number of particles with preferential arrangements, which were presumably the later nucleation sites for the growth of the flower. With controlled drying time (~8 h) in a sealed tube, large numbers of flower-like structures

(Figure 10(c)) about 500 nm in size were distributed on the silicon surface. The enlarged image Figure 10(d) from the area of Figure 10(c) shows these nano-objects possess external bonding capacity or ‘adhesiveness’ for self-assembly and self-alignment. For example, they have extending ‘arms’ (NRs or nanopetals) ideal for external connectivity (highlighted by arrows in Figure 10(d)). Fully complex geometric flowers took more than one day to develop (Figure 10(e)). Such structures comprise numerous 1D NRs or 2D nanopetals with their long-axis pointing toward the centre of each flower. Those components were arranged side-by-side and some were tightly bonded each other (highlighted by arrows in Figure 10(f)).

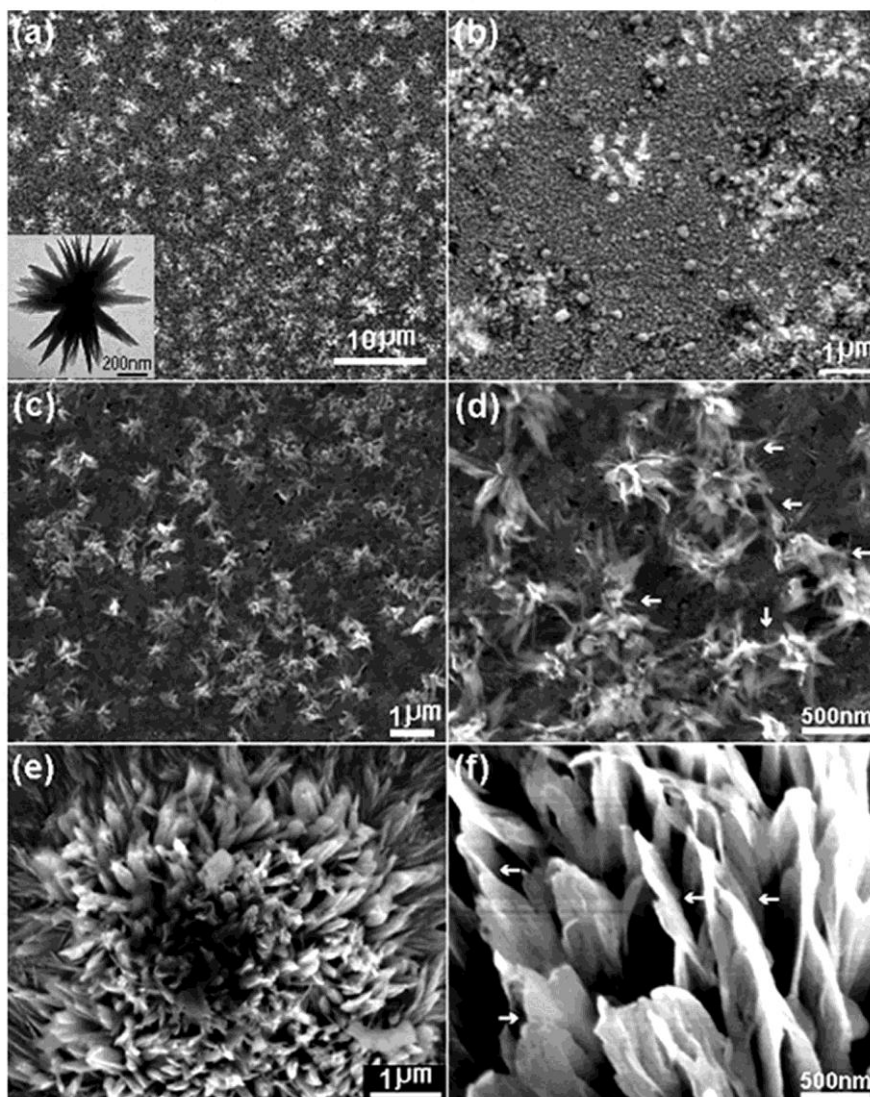


Figure 10. Time-dependent evolution of the flower-like crystal morphology at different growth stages for (a-b) 2 h, (c-d) 8 h and (e-f) 24 h, respectively. Arrows in (d) and (f) highlight the bonding components. Note that images (b), (d) and (f) are recorded at higher magnification than (a), (c) and (e), respectively. (Synthesis conditions: 35% ammonia solution, laser power 50 mJ, 12 h ablation, a flower exhibited a surface composed of NRs, where the NRs radiate outward from the centre as shown in Figure 10(a) inset. See text for discussion).

From the above discussion, it seems that the morphology of the initial stage of complex architectures (grass-like or flower like) was a small aggregate of compacted 15-20 nm-sized dense particles, which were approximately spherical in shape. Although the nucleation and growth of grass-like or flower-like carbon nitride superstructures might accompany NP fusion and self-alignment to bigger building blocks (such as NRs or nanopetals), no direct evidence was observed for this direct aggregation. Fusion and self-organization may also be associated with thermal motion of the droplets, for example, the evaporation speed, which is determined by the temperature and the flow rate of air above the surface. However, what is the driving force that controls the final hierarchical complex? The mechanism is still not fully understood. One possibility is that growth continues within the local fluid environment as long as there is substantial mobility of the seed particles for further exchange. If the process is sufficiently slow, this will continue until all the building blocks adjust to their desired (lowest energy) position. Evidence for this is that the fully developed grass-like or flower-like complexity was only observed on decreasing the evaporating rate, *i.e.* for drying times above 12 h in the later growth stage (Figure 9(e-f) and Figure 10(e-f)).

3.3.2. Influence of the Starting Seed Solution

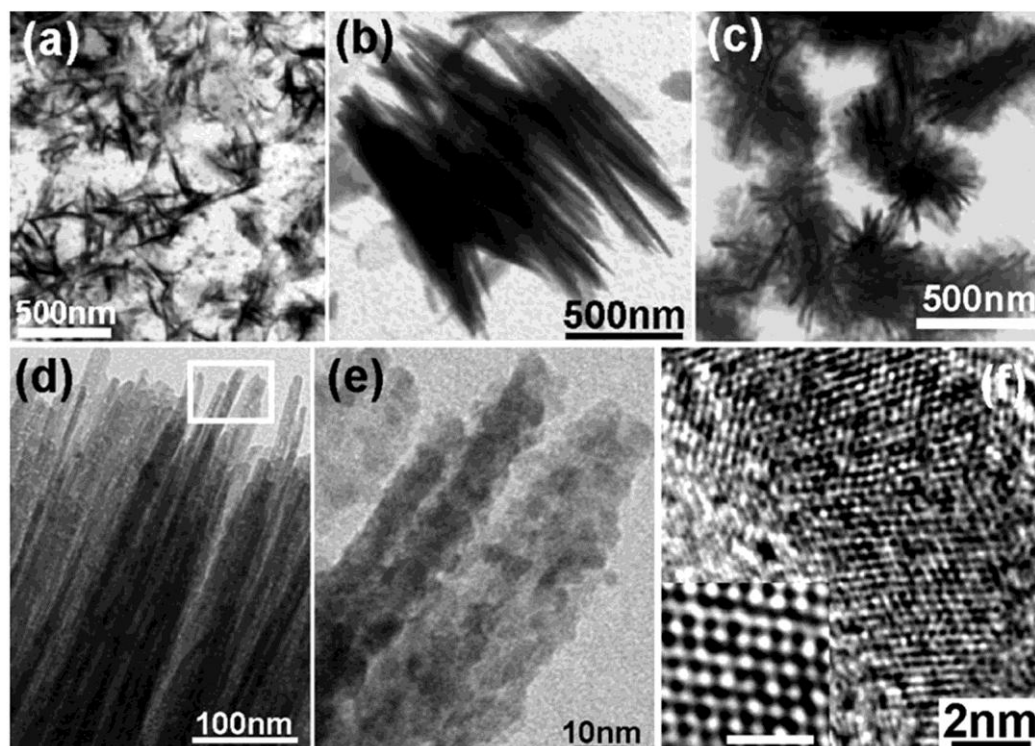


Figure 11. TEM images obtained by LP-PLA in 25% ammonia solution: (a) isolated carbon nitride NRs (50 mJ/pulse, $t = 1$ h) (b) Branched NRs (50 mJ/pulse, $t = 3$ h) (c) highly branched flowerlike architectures (100 mJ/pulse, $t = 12$ h). (d) Rod-like structures showing straight, long and sharp tips. (e) Enlarged image of the region at the top of the NRs indicated by the open box in (d). (f) HRTEM image of a single NR, the inset shows the atomic arrangement, scale bar 1 nm. (Reproduced from [30] with permission of Nova publishers).

When 35% ammonia was replaced by 25% ammonia solution, carbon nitride was still formed; however, the morphology was different under TEM observation. For low laser power (50 mJ) and short ablation time (1 h), the product contained mostly a sparse collection of isolated NRs (Figure 11(a)). With longer ablation times (3 h), the NRs started to aggregate into branched structures (Figure 11(b)), serving as the starting points (or nucleation seeds) for the subsequent growth. With increasing laser power (100 mJ) and ablation time (12 h), the concentration of NRs increased, and highly-branched flower-like architectures completely composed of NRs can be observed (Figure 11(c)). The NRs at the edge of the flower structures appeared to be protruding outward by ~ 10 nm. As shown in Figure 11(d-e), these NRs are themselves composed of a large number of smaller NPs that have packed together in an ordered arrangement to form the rod-like shapes. In particular, in the HRTEM image in Figure 11(f) taken from a single NR, the periodic lattices clearly show the atomic arrangement (Figure 11(f) inset) with no visible boundaries, and reflect the well-aligned the orientation between the NPs and the ordered NR array.

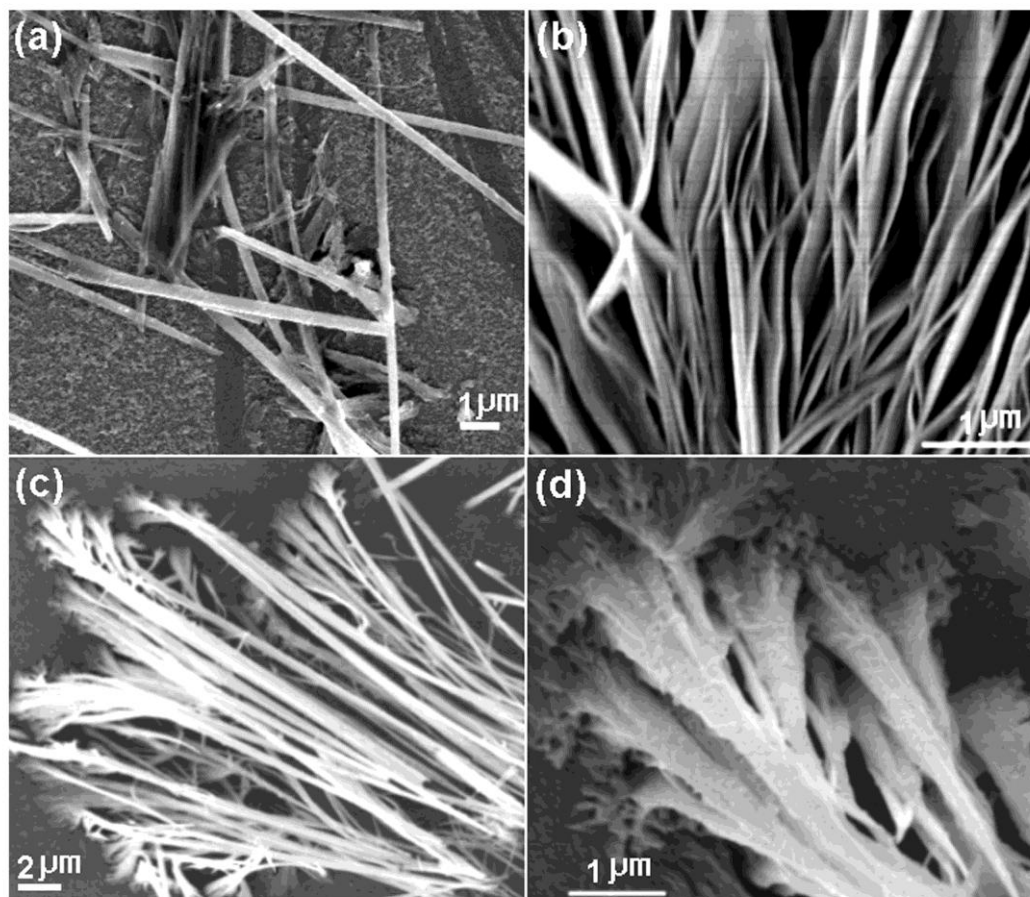


Figure 12. SEM images of different rod-like patterns obtained by drying the carbon nitride colloidal solution (a) in air (synthesis conditions: 25% ammonia solution, 50 mJ/pulse, $t = 1$ h, TEM image shows the isolated carbon nitride NRs (see Figure 11(a)). (b) in air and (c) in sealed tube (synthesis conditions: 25% ammonia solution, 50 mJ/pulse, $t = 3$ h, TEM image shows branched NRs (Figure 11(b)). Image (d) is recorded at a different magnification to (c).

The starting seed suspension can strongly influence the 2D and 3D arrangements of the nanostructures. Using the carbon nitride seed suspension prepared from ablating 25% ammonia solution, and varying the concentration and liquid evaporation rate, rod nanocrystal formation was been observed with different morphologies (Figure 12). These include irregular disordered rods (Figure 12(a)), rods with branches (Figure 12(b)), and celery-like structure (Figure 12(c-d)). One thing these morphologies have in common is that they are all originally made from rod-shaped seed particles.

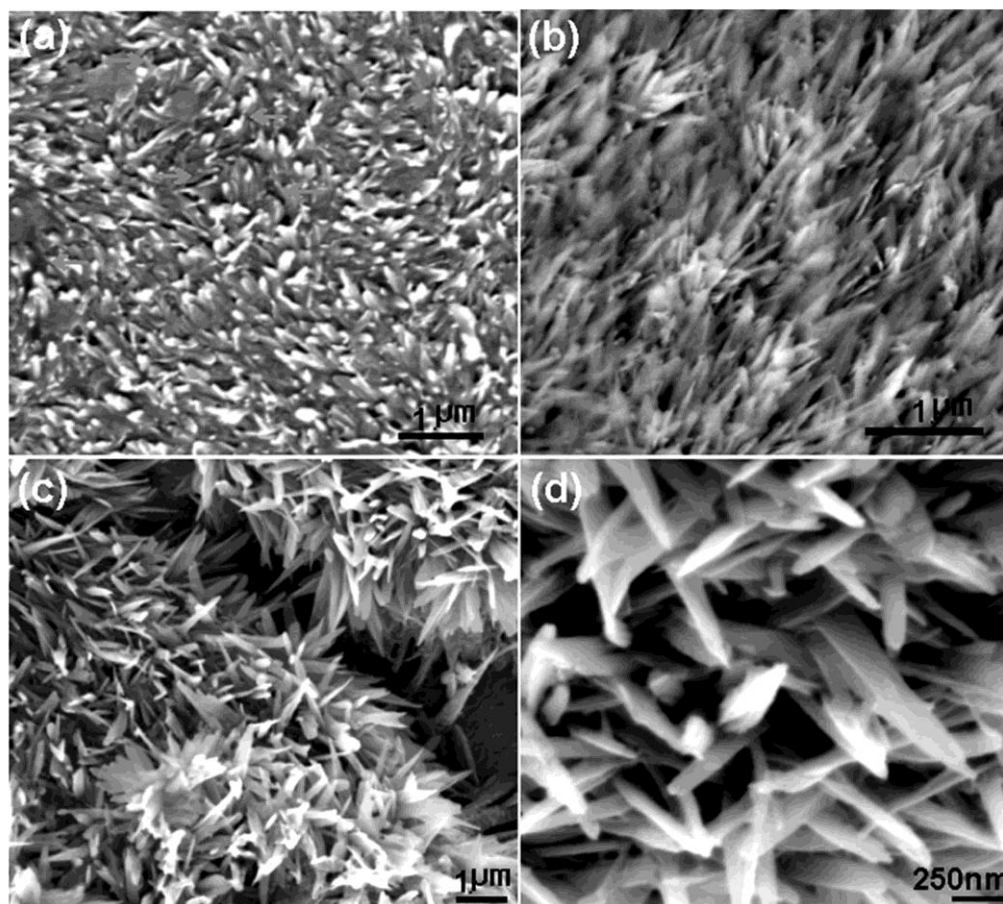


Figure 13. SEM images of carbon nitride ‘grass-like’ structures following ablation times (a) 0.5 h, (b-d) 2 h (synthesis conditions: laser power 125 mJ, 35% ammonia solution, and drying process: (a-b) drying in air and (c-d) drying in a sealed tube). Note that image (d) was recorded at high magnification than (c). Arrows in (a) point out the vacancies and cracks within the film.

We found that the size of the NPs in the initial starting suspension is also very important in determining the morphology of the carbon nitride hierarchical nanostructures. If the starting seeds were short rods (Figure 13(a)), this favoured the sticking of the NRs onto the substrate. The vacancies or cracks observed in Figure 13(a) were probably due to the fact that not enough nanocrystals were deposited on the substrate. However, if the seed solution contained sufficient number of nanocrystals with longer (about 500 nm) length, rod-rod interaction dominated and they tended to form a denser and rougher grass-like surface (Figure 13(b)). The tips of those rods were very blurred, which implies that the solvent-substrate

interaction became unstable. With longer drying time, an identical seed suspension coated on the substrate formed a homogenous grass-like film (Figure 13(c)) with plenty of radial NRs (50-200 nm in width, 1-5 μm in length). It seems that in a slow evaporation process, increasing the size and the number of the NRs is beneficial to improve the crystallinity of the individual NRs and the uniformity of the film (Figure 13(d)).

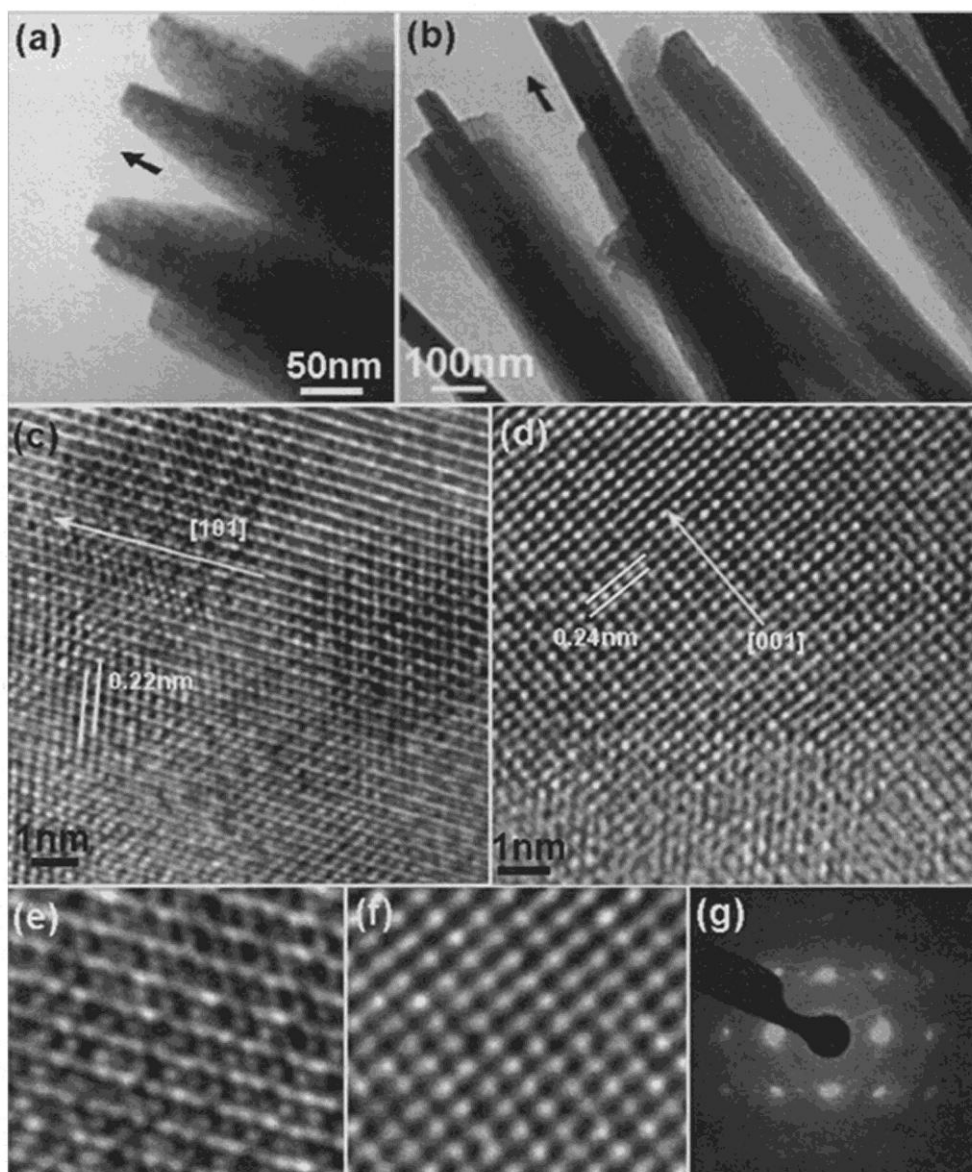


Figure 14. (a-b) TEM images of NR building blocks that form the ‘grass-like’ structures shown in Figure 13. (Synthesis conditions: laser power 125 mJ, 35% ammonia solution, 2 h ablation times, and drying process: (a) drying in air and (b) drying in a sealed tube). (c-f) HRTEM images recorded from the rods. (c) and (e) correspond to the region in (a), while (d) and (f) correspond to the region in (b). Arrows in (a-d) point to the growth direction of the NRs. (g) Microdiffraction pattern of corresponding (f) HRTEM image.

The crystallinity improvement related to the atomic and nanocrystal ordering was further observed by TEM and HRTEM. Under identical synthesis conditions, but using different drying methods, Figure 14(a) and (b) show apparent differences between those NRs subunits corresponding to Figure 13(b) and (c), respectively. When the solution is immediately dried in air (with the help of filter paper), the NRs were parallel-aligned and were 50-80 nm width and had a short length. The outline of the NRs was very blurred (Figure 14(a)). However, when drying was very slow, the NRs were very sharp, had longer length and larger width (~80-200 nm). Some NRs were overlapped and tilted away, similar to those shown in Figure 13(c-d). These results support the previous SEM observations.

From the HRTEM images shown in Figure 14(c) and (d) (which correspond to the rod area in Figure 14(a) and (b)), it was found that the crystallinity within the domain was different. However, the growth direction for those rods perfectly matched the orientation that appeared in the TEM images (highlighted by arrows in Figure 14(a) and (b)). The enlarged images of Figure 14(e) and (f) show the individual atoms and their arrangements in this small region. Figure 14(e) consists of two slightly distorted layers, which are superimposed with respect to each other, and joined in the [101] direction. Consequently, the C_3N_4 groups deviate slightly from a planar arrangement. In contrast, Figure 14(f) is more close to the idealized β - C_3N_4 structure. The atoms are linked with one edge parallel to, and one edge perpendicular to, the (001) plane, with regular ordering [43]. The micro-diffraction pattern (Figure 14(g)) from the self-aligned NPs (Figure 14(f)) shows the single-crystal type [001] zone-axis pattern. Thus, the orientation order among the NPs in the assembly was further confirmed.

4. General Discussion about Self-assembly Mechanism

Our results clearly indicate that the formation of 2D or 3D hierarchical complex architectures is evaporation-driven self-assembly [44]. Evaporation-driven self-assembly is one of the most promising techniques for practical use [45], because it is inexpensive, has a high throughput, and it is a suitable technique for both low-dimensional assemblies and long-range-ordered complex structures. Various factors in our system, such as the rate of evaporation, the starting seed suspension, and the size and the quantity of nanocrystals within the droplet, are very important to determine a well-defined self-assembly.

The formation of fully 3D carbon nitride structures was a slow process. During the evaporation process, capillary forces arise. At the edge of the meniscus, the thickness of a liquid film becomes small. The meniscus between particles has an unstable form in a thin liquid film (Figure 15). There are strong attractive interactions among the colloidal particles because of this instability. The attractive capillary force is called the 'lateral capillary force'.

When the liquid evaporation rate is high, the liquid from the bulk suspension flows to the edge of the meniscus, and other particles in the suspension are driven toward this nucleus by the resulting convective transport (Figure 16). As in our system, the droplet was composed of carbon nitride solid objects floating at the silicon substrate interface, which interact by lateral capillary forces. Such forces might direct the patterning of the wettability of the surfaces via self-assembly minimization of the interfacial free energy of the liquid-liquid interface [46]. Clearly, the morphology transformation process of NPs to hierarchical architectures requires a significant degree of mobility in the local environment [47], which could explain why the

well-defined flower-like or grass-like structures are only formed during a slow drying process. Similarly, the diffusion of the building blocks and the interconnection between the larger structures are also related to such motion of the liquid flux. A high concentration of starting seed suspension containing more components within the droplet may induce more interaction between the nanocrystals and thereby increase the chance for the self-organization of aggregates in the later stages.

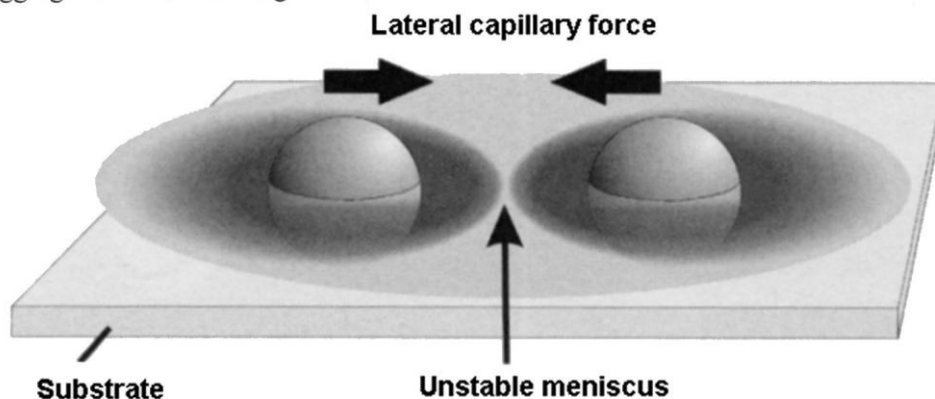


Figure 15. Schematic diagram of the lateral capillary force caused by an unstable meniscus. (Reproduced from [48] with permission of Wiley interscience).

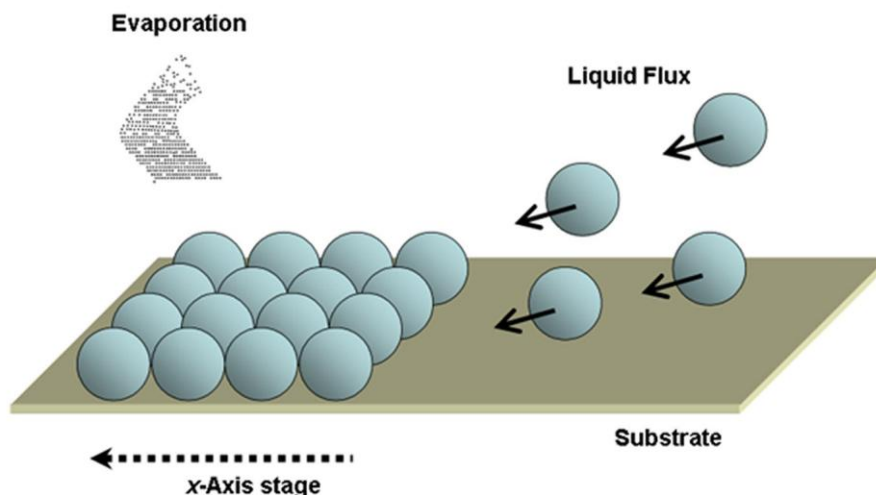


Figure 16. Schematic diagram of evaporation-driven self-assembly.

In self-assembly, the molecular structure determines the structure of the assembly [49]. Therefore, it is believed that the self-assembly into functional structures can be fabricated through design of the various components. Our results in section 3.3.2 have shown that the different shape of the starting components leads to the formation of different structurally defined aggregates. For example, the rod-like seeds generated rod-branches (Figure 12) or grass-like structures (Figure 13) depending on the conditions, where the original shape of the components remained intact. The more complicated the shape, the more difficult it is to predict the final form of any aggregate. Further in-depth understanding of such phenomenon is required in future research.

5. Conclusions

The formation and morphological evolution of 2D or 3D carbon nitride hierarchical complex structures was studied in this chapter. A two-step strategy was developed to control the final well-defined superstructures. In the first step, carbon nitride seed suspensions were prepared by liquid-phase pulsed laser ablation. In the second stage the chosen seed suspension was deposited onto a silicon substrate. Via controlling the rate of evaporation, the starting seed suspension, and the size and the quantity of nanocrystals within the droplet, it was possible to create dense nanospheres, highly-symmetric flowers, and uniform grass-like structures, respectively.

Because of the mobility in the local environment, the smaller building blocks (NPs) appeared to be mobile with respect to the larger structures (flowers), and diffused outward from the centre with longer drying times. Such diffusion created different degrees of hollow structure, including core-shell, semi-hollow, and hollow organization, which may find applications in new technological areas. In addition, interconnection between the larger structures was also observed for slow evaporation processes. For dense nanospheres, the fusing of the pristine nanospheres was weak and they were easily separated. However, the nanoflowers with many protruding NRs had sufficient capacity for the component NRs to occupy the spaces within the nanoflowers and fuse the flowers together more strongly.

From studies of the dynamics of self-assembly formation, it seems that the morphology of the initial stage of the complex architectures (grass-like or flower-like) was small aggregates of compacted 15-20 nm-sized dense spherical particles. The self-organization in the later stage may be associated with thermal motion of the droplets, for example, the evaporation speed. Although the mechanism is still not fully understood yet, our experiments which compared drying time and starting seed suspension indicated that self-assembly into functional structures can be achieved through the design of the various components. A slow drying process will favour an increase in the structural complexity.

The formation of 2D or 3D hierarchical complex architectures in this work seems to be an evaporation-driven self-assembly process. The beauty of this approach is its simplicity and efficiency. If combined readily with micrometre-scale film patterning strategies, such as microcontact printing [50], direct writing, or lithography, it may provide a convenient pathway to the formation of functional hierarchical devices. By varying the design of the building blocks, materials combination, interfacial chemistry, and confining dimensions, we should expect to discover new materials properties.

References

- [1] Whitesides, G. M.; Boncheva, M. *Proc. Natl Acad. Sci. USA*, 2002, 99, 4769-4774.
- [2] Hamley, I. W. *Angew. Chem. Int. Ed.*, 2003, 42, 1692-1712.
- [3] Yin, J. S.; Wang, Z. L. *Handbook of Nanophase and Nanostructured Materials*, Volume 4, Kluwer Academic/Plenum Publishers, Tsinghua University Press, New York, 2003, p. 174.
- [4] Tang, Z. Y.; Kotov, N. A.; Giersig, M. *Science*, 2002, 297, 237-240.
- [5] Liu, B.; Zeng, H. C. *J. Am. Chem. Soc.*, 2005, 127, 18262-18268.

- [6] Kempa, K.; Kimball, B.; Rybczynski, J.; Huang, Z. P.; Wu, P. F.; Steeves, D.; Sennett, M.; Giersig, M.; Rao, D. V. G. L. N.; Carnahan, D. L.; Wang, D. Z.; Lao, J. Y.; Li, W. Z.; Ren, Z. F. *Nano Lett.* 2003, 3, 13-18.
- [7] Duan, X. F.; Lieber, C. M. *Adv. Mater.*, 2000, 12, 298-302.
- [8] Sun, Y.; Fuge, G. M.; Fox, N. A.; Riley, D. J.; Ashfold, M. N. R. *Adv. Mater.*, 2005, 17, 2477-2481.
- [9] Yang, H. G.; Zeng, H. C. *J. Phys. Chem. B*, 2004, 108, 3492-3495.
- [10] Mirkin, C. A.; Letsinger, R. L.; Mucic, R. C.; Storhoff, J. J. *Nature*, 1996, 382, 607-609.
- [11] Sun, Y. G.; Gates, B.; Mayers, B.; Xia, Y. N. *Nano Lett.*, 2002, 2, 165-168.
- [12] Li, Y. D.; Li, X. L.; Deng, Z. X.; Zhou, B. C.; Fan, S. S.; Wang, J. W.; Sun, X. M. *Angew. Chem. Int. Ed.*, 2002, 41, 333-335.
- [13] Motte, L.; Billoudet, F.; Pileni, M. P. *J. Phys. Chem.* 1995, 99, 16425-16429.
- [14] Maillard, M.; Motte, L.; Pileni, M. P. *Adv. Mater.* 2001, 13, 200-204.
- [15] Liu, B.; Zeng, H. C. *J. Am. Chem. Soc.*, 2004, 126, 8124-8125.
- [16] Petit, C.; Legrand, J.; Russier, V.; Pileni, M. P. *J. Appl. Phys.*, 2002, 91, 1502-1508.
- [17] Ngo, A. T.; Pileni, M. P. *Adv. Mater.*, 2000, 12, 276-279.
- [18] Liu, J. P.; Huang, X. T.; Li, Y. Y.; Sulieman, K. M.; He, X.; Sun, F. L. *J. Mater. Chem.*, 2006, 16, 4427-4434.
- [19] Liu, B.; Zeng, H. C. *J. Am. Chem. Soc.*, 2004, 126, 16744-16746.
- [20] Lu, Q. F.; Zeng, H. B.; Wang, Z. Y.; Cao, X. L.; Zhang, L. D. *Nanotechnology*, 2006, 17, 2098-2104.
- [21] Yang, L.; May, P. W.; Yin, L.; Brown, R.; Scott, T. B. *Chem. Mater.*, 2006, 18, 5058-5064.
- [22] Yang, L.; May, P. W.; Yin, L.; Scott, T. B.; Smith, J. A.; Rosser, K. N. *Nanotechnology*, 2006, 17, 5798-5804.
- [23] Yang, L.; May, P. W.; Yin, L.; Huang, Y. Z.; Smith, J. A.; Scott, T. B. *Nanotechnology*, 2007, 18, 335605 (5pp).
- [24] Yang, G. W. *J. Prog. Mater. Sci.*, 2007, 52, 648-698.
- [25] Wang, J. B.; Zhang, C. Y.; Zhong, X. L.; Yang, G. W. *Chem. Phys. Lett.*, 2002, 361, 86-90.
- [26] Sounart, T. L.; Liu, J.; Voigt, J. A.; Hsu, J. W. P.; Spoerke, E. D.; Tian, Z.; Jiang, Y. B. *Adv. Funct. Mater.*, 2006, 16, 335-344.
- [27] Liu, A. Y.; Cohen, M. L. *Science* 1989, 245, 841-842.
- [28] Li, J.; Cao, C. B.; Hao, J. W.; Qiu, H. L.; Xu, Y. J.; Zhu, H. S. *Diamond Relat. Mater.*, 2006, 15, 1593-1600.
- [29] Yang, L.; May, P. W.; Huang, Y. Z.; Yin, L. *J. Mater. Chem.*, 2007, 17, 1255-1257.
- [30] Yang, L.; May, P. W.; Yin, L. *Nanotechnology Research Developments*, Nova Publishers, Hauppauge, NY, 2007.
- [31] Sylvestre, J. P.; Kabashin, A. V.; Sacher, E.; Meunier, M. *Appl. Phys. A*, 2005, 80, 753-758.
- [32] Pyatenko, A.; Shimokawa, K.; Yamaguchi, M.; Nishimura, O.; Suzuki, M. *Appl. Phys. A*, 2004, 79, 803-806.
- [33] Rakshit, R. K.; Budhani, R. C. *J. Phys. D*, 2006, 39, 1743-1748.
- [34] Wang, J. B.; Lei, J. L.; Wang, R. H. *Phys. Rev. B*, 1998, 58, 11890-11895.
- [35] Brinker, C. J.; Lu, Y. F.; Sellinger, A.; Fan, H. Y. *Adv. Mater.*, 1999, 11, 579-585.

-
- [36] Liu, B.; Zeng, H. C. *Small*, 2005, 1, 566-571.
- [37] Penn, R. L.; Banfield, J. F. *Science*, 1998, 281, 969-971.
- [38] Lu, T. R.; Kuo, C. T.; Yang, J. R.; Chen, L. C.; Chen, K. H.; Chen, T. M. *Surf. Coat. Tech.*, 1999, 115, 116-122.
- [39] Zimmerman, J. L.; Williams, R.; Khabashesku, V. N.; Margrave, J. L. *Nano Lett.*, 2001, 1, 731-734.
- [40] Likhacheva, A. Y.; Paukshtis, E. A.; Seryotkin, Y. V.; Shulgenko, S. G. *Phys. Chem. Miner.*, 2002, 29, 617-623.
- [41] Liu, A. Y.; Cohen, M. L. *Phys. Rev. B* 1990, 41, 10727-10734.
- [42] Zhang, Z. P.; Shao, X. Q.; Yu, H. D.; Wang, Y. B.; Han, M. Y. *Chem. Mater.*, 2005, 17, 332-336.
- [43] Wang, C. M.; Pan, X. Q.; Rühle, M.; Riley, F. L.; Mitomo, M. *J. Mater. Sci.*, 1996, 31, 5281-5298.
- [44] Maenosono, S.; Okubo, T.; Yamaguchi, Y. *J Nanoparticle Res.*, 2003, 5, 5-15.
- [45] Salamanca, J. M.; Ciampi, E.; Faux, D. A.; Glover, P. M.; McDonald, P. J.; Routh, A. F.; Peters, A. C. I. A.; Satguru, R.; Keddie, J. L. *Langmuir*, 2001, 17, 3202-3207.
- [46] Bowden, N.; Terfort, A.; Carbeck, J.; Whitesides, G. M. *Science*, 1997, 276, 233-235.
- [47] Li, M. *PhD thesis*, University of Bristol, 2000, pp. 132.
- [48] Matsushita, S.; Onoue, S. Y. *Three-dimensional self-assemblies of nanoparticles, Nanocrystals Forming Mesoscopic Structures*, Pileni M P (ed.), Wiley-VCH Verlag GmbH & Co. KGaA, 2005, Weinheim, Germany, p.140.
- [49] Whitesides, G. M.; Simanek, E. E.; Gorman, C. B. *Nano Advanced Study Institute on Chemical Synthesis: Gnosis to Prognosis*, eds. Chatgililoglu C, Snieckus V, 1996, Kluwer, Dordrecht, Netherlands, pp. 565-588.
- [50] Jeon, N. L.; Finnie, K.; Branshaw, K.; Nuzzo, R. G. *Langmuir*, 1997, 13, 3382-3391.